APPLIED SCIENCES AND ENGINEERING

The Temple Scroll: Reconstructing an ancient manufacturing practice

Roman Schuetz[1]*, Janille M. Maragh[2]*, James C. Weaver[3], Ira Rabin[4,5], Admir Masic[2]†

The miraculously preserved 2000-year-old Dead Sea Scrolls, ancient texts of invaluable historical significance, were discovered in the mid-20th century in the caves of the Judean desert. The texts were mainly written on parchment and exhibit vast diversity in their states of preservation. One particular scroll, the 8-m-long Temple Scroll is especially notable because of its exceptional thinness and bright ivory color. The parchment has a layered structure, consisting of a collagenous base material and an atypical inorganic overlayer. We analyzed the chemistry of the inorganic layer using x-ray and Raman spectroscopies and discovered a variety of evaporitic sulfate salts. This points toward a unique ancient production technology in which the parchment was modified through the addition of the inorganic layer as a writing surface. Furthermore, understanding the properties of these minerals is particularly critical for the development of suitable conservation methods for the preservation of these invaluable historical documents.

INTRODUCTION

Ancient texts, known collectively as the Dead Sea Scrolls (DSS), were discovered in the middle of the last century and are certainly some of the most treasured objects of cultural heritage. The DSS were miraculously preserved in the natural limestone and man-made marl caves of the Judean desert, and the main collections are held in the Israel Antiquity Authority, the Shrine of the Book, and Jordan. Apart from having inherent textual value, the DSS also carry historical information related to the materials processing technologies that were used to produce them. A detailed understanding of these ancient technologies could be used for forgery identification purposes and for the development of modern antiquity-inspired, collagen-based materials (*1*).

Most of the DSS were written on animal skin–based material that can be roughly described as a hybrid of parchment and leather. Similar to medieval practices, production of the writing surfaces from the skins of cattle, sheep, and goats included four main steps: de-hairing, thinning, drying under tension, and finishing. However, in contrast to medieval and modern techniques, the first step (i.e., de-hairing) was conducted without a lime solution, which led to a higher content of fats in the processed skins (*2*). The de-hairing in the case of DSS involved an enzymatic treatment, which was likely carried out by application of fermented grains. In addition, vegetable tannins were occasionally applied to the surface during the final stage of skin processing (*3*, *4*).

This general description of the DSS production process, however, lacks the specific characteristics of the materials used for the drying and finishing steps. It is known that in the case of Middle Age parchments, chalk and powdered pumice were applied to the flesh side to aid in the cleaning and drying of the de-haired skin (*5*), but this was not the case for the DSS. It is also known that aluminum sulfate salts, known as alum [$MAl(SO_4)_2{\cdot}12H_2O$, M = Na, K, NH_4^+], have been used throughout antiquity for tawing skins to produce soft, white leather of excellent quality (*6*). In the case of extremely thin parchments from the DSS collection, which served as a writing surface for phylacteries, the production involved splitting of the de-haired skin into two parts, the grain split (carrying a follicle pattern) and the flesh split (*7*). It appears, however, that the practice of manually splitting skins did not exist in the Middle Ages, when lime was universally used as the de-hairing agent.

In a recent study, an integrated methodology for determining the original and acquired properties of the DSS has been developed (*8*). Using a combination of x-ray, Fourier transform infrared (FT-IR), and Raman techniques, it was possible to identify the organic and inorganic phases present in the scrolls. It was shown that the organic (parchment) and inorganic (sediments from the caves) phases of the ancient fragments were not completely intermixed and could be spatially resolved. In most of the cases studied, the mineral deposits that were detected on the surface of the scrolls could be linked to those of the caves. In a smaller number of fragments, however, the surface was coated with a thin mineral layer that presumably originated from the parchment production process. These investigations led to the conclusion that the skin-based writing surfaces of the DSS could be roughly grouped into three different categories: leather parchments; parchments of various shades of brown, which were tanned using the "Eastern" practice; and light-colored untanned parchments, which were produced using the "Western" practice (*9*). The similarities of the second and third of these categories of the DSS to Babylonian documents from the 5th century BCE and early Greek parchments led to the hypothesis that Eastern and Western parchment production technologies coexisted at the time of the production of the DSS.

Among all the DSS, there is one particular document, the Temple Scroll (TS) ($11QT^a$) from the Israel Museum's collection, which is especially notable because of its physical appearance (Fig. 1, A and B). The TS is written on a bright ivory-colored parchment that measures 8.148 m in length, and its thickness hardly exceeds 0.1 mm. Its recovery history is more complicated than that of other scrolls in the collection. Allegedly, a group of Bedouins found it wrapped in cloth in a jar in 1956 in Cave 11 of Qumran and then sold it to an antiquities dealer who replaced the original encasement with cellophane and then transferred it from the jar into a shoebox that he hid under the floor in his home. When scholars finally accessed the scroll some 11 years later, it was severely damaged by moisture, particularly on its outer sheets and upper edge (*10*). Previous studies have confirmed that the TS was retrieved from Cave 11 (*11*).

[1]D-REAMS Radiocarbon Laboratory, Weizmann Institute of Science, Rehovot, Israel. [2]Department of Civil and Environmental Engineering, Massachusetts Institute of Technology, Cambridge, MA 02139, USA. [3]Wyss Institute for Biologically Inspired Engineering, Harvard University, Cambridge, MA 02138, USA. [4]Bundesanstalt für Materialforschung und -prüfung, Berlin, Germany. [5]Centre for the Study of Manuscript Cultures, Hamburg University, Hamburg, Germany.
*These authors contributed equally to this work.
†Corresponding author. Email: masic@mit.edu

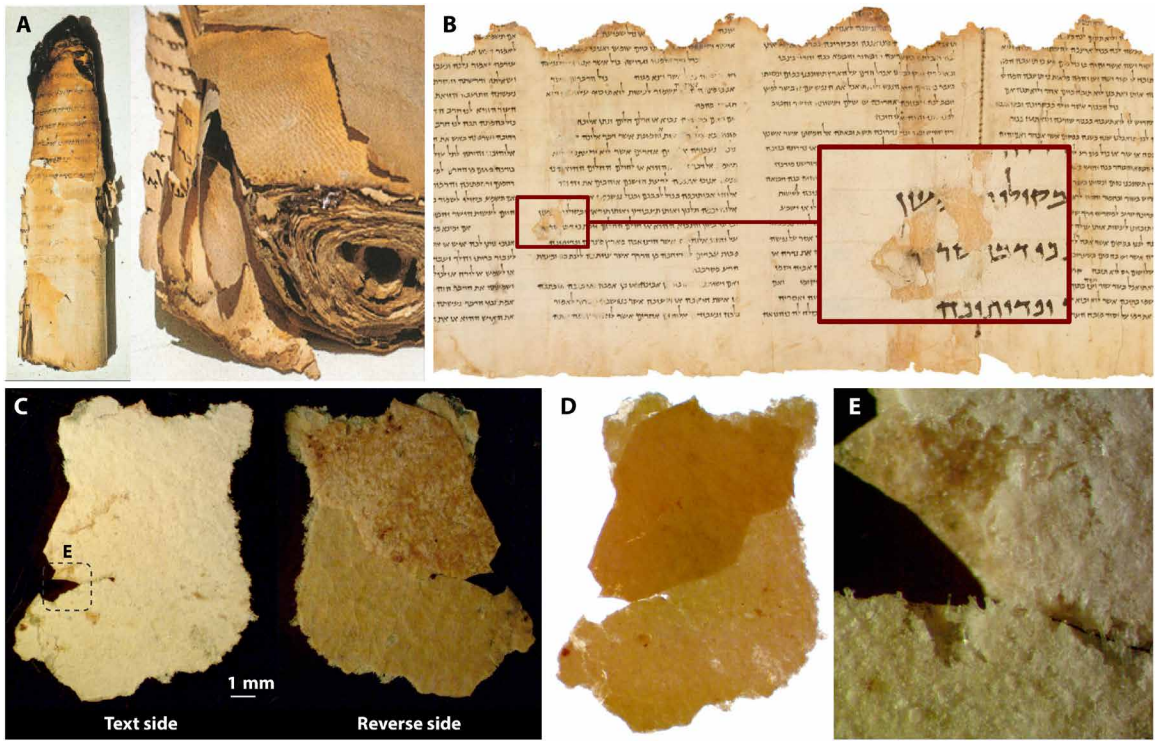

Fig. 1. Light microscopy of the TS, showing its layered structure from the macroscale to the microscale. (**A**) Photographs of the TS showing damage to the upper part of the scroll (left). The reverse side of the preserved section (right) shows the follicle pattern of the hairs removed from the skin, which indicated that the text is written on the flesh side of the treated skin (*13*). [(A): Courtesy of the Estate of Yigael Yadin.] (**B**) Column 54 of the unrolled TS (*29*). The enlarged inclusion (inset) shows that some parts of the bright, text-carrying inorganic layer have been detached. [(B): Photo credit: The Israel Museum, Jerusalem.] (**C**) Fragment of TS showing inorganic layer on text side (left) and reverse side (right). The organic layer has partially detached, revealing the inner surface of the inorganic layer. (**D**) The same fragment in light transmittance from the back differentiating the thinner lower part, where the detachment has occurred from the thicker upper part. (**E**) Enlarged optical micrograph of the boxed region in (C).

Immediately after its purchase by the State of Israel, the unrolling of the tightly wound scroll was conducted in accordance with the Plenderleith method (*12*). This involved the humidification of the scroll up to 100% relative humidity with subsequent short freezing to arrest the gelatinization process. Thus, the first visual description of the scroll by Y. Yadin depicted its state after unrolling and the reassembly of previously detached fragments. Yadin believed that the nonuniform state of preservation, which varied greatly from sheet to sheet, resulted from a nonuniform treatment of the parchment in antiquity (*10*). Furthermore, some of the text was found only as a mirror image imprint on the verso of the columns with which it was in contact, leaving blank surfaces behind. This type of text transfer occurred indiscriminately throughout the scroll and did not seem to be correlated with the state of degradation (*13*). X-ray diffraction and FT-IR studies of the TS parchment collagen showed high degrees of degradation juxtaposed with apparently good states of preservation (*14*, *15*). More recently, through an investigation of individual collagen fibers within the TS fragments using polarized μ–Raman spectroscopy, well-preserved collagen was detected beneath a detached outer inorganic layer (*16*).

In this work, the chemistry of the inorganic layer of an unprepared fragment of the TS was studied using μ–x-ray fluorescence (μXRF), energy-dispersive spectroscopy (EDS), and Raman spectroscopy. The results demonstrate the presence of a complex mixture of evaporitic salts as the major component of the inorganic layer on which the text was written. The mineral phases that were detected on the TS are typical for nonmarine evaporitic mineral deposits, and the findings of this work point to a specific technique that was used to produce the TS.

RESULTS

Whereas most of the DSS are quite dark in color, a small number among them, including the TS, are light colored (*17*). In addition to its bright appearance, the TS exhibits a multilayered structure with the text written on the ivory-colored inorganic layer that covers the flesh side of the skin. The reverse side of the TS reveals the hair side of the processed skin, which is more yellow in appearance. The hair follicle pattern visible on the reverse side of the scroll (Fig. 1A) indicates that the text was at least partially written on the flesh side of the parchment. On the text side (Fig. 1C, left), regions of the inorganic layer are often missing, exposing the yellowish collagenous layer beneath. Similarly, there are regions where the detached inorganic layer is preserved. The patches of the detached text-containing inorganic layer that were found stuck to the reverse side of the scroll were an unexpected result in the study of the TS (*10*).

The uninscribed fragment of the TS presented here (Fig. 1) includes regions where the yellowish organic layer is missing, and the resulting differences in thickness throughout the sample can be seen in the light transmittance image in Fig. 1D. The multilayered structure is also clearly visible in the enlarged optical micrograph in Fig. 1E corresponding to the region of interest (ROI) in Fig. 1C (left). A

schematic representation of the fragment stratigraphy can be found in fig. S1.

μXRF and EDS study of the TS

The TS is a notably heterogeneous material (Fig. 2A), so to better characterize this complexity, we conducted μXRF and EDS analyses on both sides of the TS fragment to investigate its elemental composition. The μXRF sum spectra of two ROIs (Fig. 2B) show a complex inorganic layer composition with major elements that include Na, Mg, Al, Si, P, S, Cl, K, Ca, Mn, Fe, and Br. The K-line μXRF element distribution maps of some of these elements, plotted in Fig. 2C, show that the major elements Na, Ca, S, Mg, Al, Cl, and Si are distributed throughout the entire fragment. Al appears to be fairly evenly distributed throughout the fragment, but this map may be unreliable because of the close proximity of the K-line of Al to the L-line of Br. The K and Fe maps are likely associated with contaminants rather than with intentional additives during the TS production process.

Although certain elements, such as Mn, Fe, and Br, appear to be more concentrated in the thicker regions of the fragment where the organic layer was not detached, it should be noted that this could be an artifact due to sample thickness. Lighter elements would only be detected near the surface because of the absorption of their lower

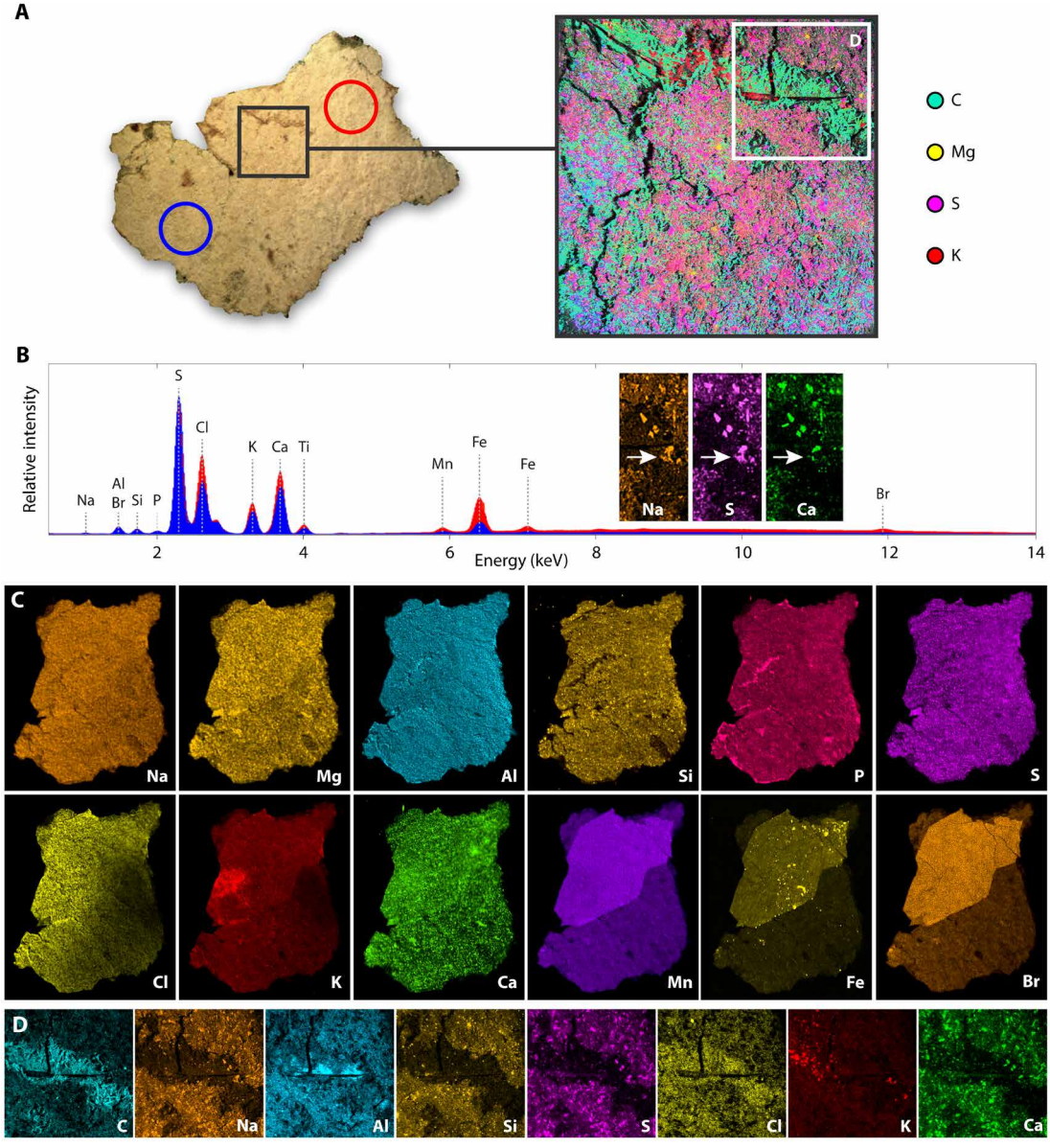

Fig. 2. Large-scale μXRF and EDS characterization of the text-containing side of the TS. (**A**) The text-containing surface of the TS (optical image, left) is extremely heterogeneous, as demonstrated in the large-area multielement EDS map (right). (**B**) Large-area μXRF elemental averages demonstrate clear compositional differences between the blue circled region, which largely encompasses the inorganic overlayer, and the red circled region, which includes both the mineral overlayer and the underlying collagenous base material. (**C**) μXRF elemental distribution maps of the 12 most evident relevant elements. (**D**) EDS elemental maps of the ROI area indicated on the multielement EDS map in (A). From these EDS measurements and those shown in the small Na, S, and Ca elemental maps [(B), inset] of cropped regions of (D), we observe some elemental clusters where the particles (denoted by the arrows) contain Na and S but very little Ca. Other Ca-containing particles without Na and/or S were also identified.

energy characteristic x-rays within the sample, whereas higher energy x-rays from heavier elements would be detected throughout the entire thickness of the fragment.

The μXRF element maps may be studied in conjunction with the distribution of cracks and small detachments throughout the inorganic layer to improve the understanding of the phases associated with the different elements. Na and Cl show a similar distribution throughout the entire measured area, i.e., the regions of the fragment that still have the organic layer attached have a greater Na and Cl concentration. In contrast to Na's more uniform coverage of the sample, the Cl distribution map does not follow the pattern of cracks and small detachments in the inorganic layer. The Na-Cl distribution correlation maps may thus indicate the presence of sodium chloride (NaCl) only inside the organic skin layer, which is a known remnant from the DSS skin/parchment processing process (*3*, *6*, *18*).

To quantify the elements of interest on the surface of the fragment, we conducted scanning electron microscopy (SEM)–EDS on the ROI illustrated by the dashed box on the multicolor EDS map in Fig. 2A. SEM-EDS allows high lateral spatial resolution due to the comparatively smaller depth penetration of the electrons. Low-vacuum SEM was used for this purpose because it minimizes vacuum-induced damage and allows the elemental mapping of noncoated (nonconductive) samples. The EDS element maps (Fig. 2D) show particles in the inorganic layer ROI that predominantly contain sodium, sulfur, and calcium. Silicon was also detected in the inorganic layer but not in the Na-S-Ca particles found on the surface of the inorganic layer, and Al and Cl were detected at higher concentrations between the particles and in the organic material. The sodium, sulfur, and calcium element maps (inset in Fig. 2B) show clear correlation between these three elements, and the arrows indicate the particles in which sodium and sulfur, but little calcium, were observed.

Raman spectroscopy study of the TS

From the μXRF and EDS studies, it is clear that the inorganic layer contains particles rich in sodium, calcium, and sulfur, along with other independent mineral phases. However, because the chemical bonding and phase characterization cannot be fully realized using μXRF and EDS, Raman spectroscopic investigations were also performed (Fig. 3). To reduce the background fluorescence typically observed in Raman spectra of the DSS, we used low-energy excitation wavelengths. First, FT-Raman operating at an excitation wavelength of 1064 nm was used to collect average spectra from the TS fragment from very large spot sizes (400 μm in diameter) (Fig. 3A). Both spectra show three main components: a sulfate double peak at 987 and 1003 cm^{-1}, a nitrate peak at 1044 cm^{-1}, and the proteinaceous contribution typical of collagen or gelatin.

The spatial resolution of FT-Raman did not allow the differentiation of the inorganic particles and the collagen fibers, so confocal Raman spectroscopy measurements were performed using a near-infrared 785-nm laser excitation on the same fragment. Spectra for the collagen fibers (spectrum I) and inorganic particles (spectra II and III) are reported in Fig. 3B. The collagen fiber spectrum includes the characteristic nitrate peak at 1043 cm^{-1}, which can be assigned to the ν_1 vibration of the NO_3^- ion in NH_4NO_3 (*19*).

Spectrum II, which was collected on a Na-S-Ca–containing particle of the inorganic layer, is characterized by two peaks in the sulfate (SO_4^{2-}) region (987 and 1007 cm^{-1}). The intensity ratio of these two peaks varied from particle to particle throughout the TS fragment. The variability in the Na-S-Ca particles suggests that the particles are composed of mixtures of various sulfate-containing minerals in different proportions. Comparison of the spectral features of these particles with spectra of reference samples of inorganic salts containing SO_4^{2-} ions, namely, glauberite [$Na_2Ca(SO_4)_2$], gypsum ($CaSO_4{\cdot}2H_2O$), and thénardite (Na_2SO_4), did not yield satisfactory matches (fig. S2). Raman peaks of the air-dried, synthetic Na_2SO_4 and $CaSO_4$ aqueous mixture, which are located around 450 and 630 cm^{-1} also differ from the TS spectrum II (Fig. 3B). However, drying this synthetic mixture by fast evaporation at 250°C resulted in different evaporate particles, which in some cases yielded Raman spectra similar to those of the TS in the sulfate regions (fig. S2).

Spectrum III in Fig. 3 is associated with very small particles in the inorganic layer that are about 5 to 15 μm in diameter (distribution shown in Fig. 3C). These particles showed very intense Raman scattering using an excitation wavelength of 785 nm. The characteristic triplet spectral signature at 1200, 1265, and 1335 cm^{-1} reflects vibrational units of the type "Na_2-X." This triplet is characteristic of sulfates that contain Na and is often detected in the minerals thénardite and glauberite (fig. S3).

EDS study of the TS and Cave 4 fragments

A multidetector EDS system was also used to collect large-area elemental maps of ROIs on both the text and reverse sides of the TS fragment (Fig. 4). Backscattered SEM (BS-SEM) imaging of the brighter text-containing side (Fig. 4B) and the darker reverse side (Fig. 4C) revealed an extremely heterogeneous composition. In the vicinity of a large crack on the text-containing side (Fig. 4B), for example, clear differences in electron density could be seen between the inorganic overlayer and the underlying collagenous material.

The major elements present in the fragment (Ca, Cl, Fe, K, Mg, Na, P, S, Si, C, and O) were then quantified by atomic percent. Note that the results from the quantification of C and O are unreliable because of the low energies of their characteristic x-rays and the ambient chamber concentrations of O under the low-vacuum conditions under which the data were collected; hence, these results were excluded from any further analysis. The ratios of the three elements of interest from the aforementioned μXRF, EDS, and Raman studies of the particles within the inorganic layer (i.e., Na, Ca, and S) at each point of the 512 pixel–by–512 pixel measured area are shown on ternary axes in Fig. 4. Ternary density plots (Fig. 4, A and D) show the relative density of points on the diagrams, as described by the color bar on the right of Fig. 4D. Both ternary plots show that the ratios of calcium to sodium to sulfur at each pixel of the measured areas on both the text side and the reverse side lie between the theoretical ternary diagram locations for glauberite [red dot, measured chemistry: $Na_{1.90}Ca_{1.15}(S_{0.99}O_4)_2$ (*20*)] and thénardite [green dot, measured chemistry: Na_2SO_4].

The quantified EDS data were then clustered with respect to a set of the major elements (excluding C and O) using the fuzzy c-means clustering algorithm (Fuzzy Logic Toolbox, MATLAB R2018a) to visualize the distribution of different phases present on the text and reverse sides of the TS fragment. These results were then used to determine the most likely division of the 512^2 data points of each dataset into a predefined number of clusters. The data for the text side were divided into three clusters, and the data for the reverse side were divided into four. The clustering results are reported as both overlapping clusters on ternary axes (Fig. 4, E and H) and as distributions maps (Fig. 4, F and G). The clustering results show the distribution of the dark, organic material on the reverse side of the

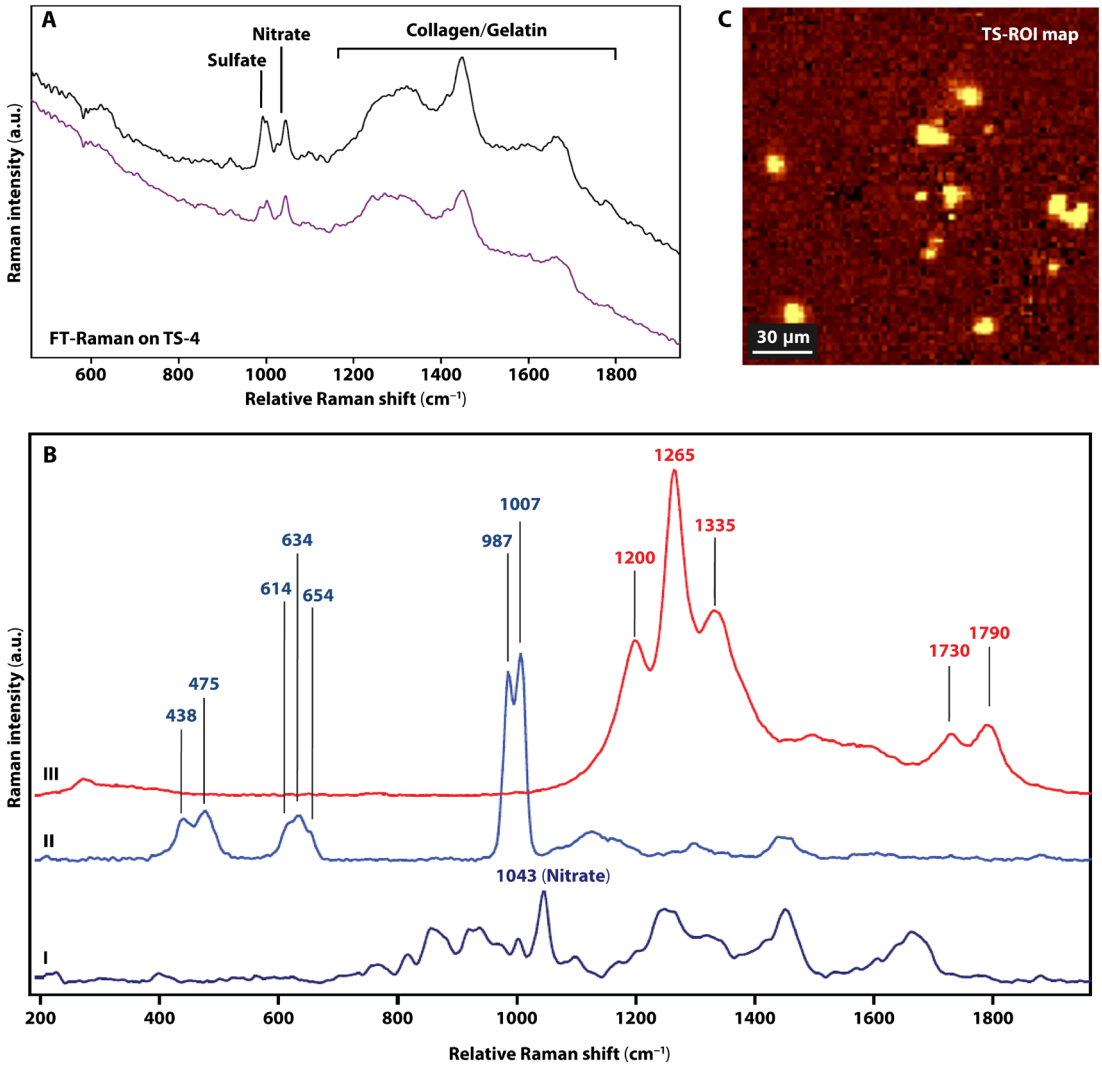

Fig. 3. Raman spectra for the composite materials of the TS. (**A**) FT-Raman spectra of two regions of the text side of a TS fragment. a.u., arbitrary units. (**B**) Confocal micro-Raman at 785-nm spectra of the TS composites. I: Collagen spectrum; collagen spectra inside the TS always contain a nitrate peak at 1043 cm^{-1}. II: Sulfate spectrum of particles with Na, S, and Ca constituents. III: Unidentified particles distributed throughout the inorganic surface layer, which yielded very resonant Raman signals with 785-nm laser excitation. (**C**) Distribution map of the particles on the surface of the inorganic layer, which were resonant for Raman excitation at 785 nm.

TS (Fig. 4K, blue) and where the cracks in the inorganic layer on the text side expose the collagen layer beneath it (Fig. 4J, yellow). Note that the colors assigned to the clusters for the text side do not correspond to the colors assigned to the clusters on the reverse side.

To show the distribution of Na-Ca-S ratios, the points on the ternary diagrams were colored as a mixture of three colors (RGB) according to their ternary positions (Fig. 4, I and L), in which the top vertex (sulfur) is green, the left vertex (calcium) is red, and the right vertex (sodium) is blue. The same colors were then used to identify the corresponding pixels in the measured area (Fig. 4, J and K). The resulting blue-green distribution maps demonstrate a high sodium, low calcium, and moderate sulfur content throughout both the text side and the reverse side of the TS.

The same methodology was also used to show the distribution of Na-Ca-S for another region of the text side of the TS fragment and several regions of the front and reverse sides of three scroll fragments obtained from the 4Q cave in Qumran (R-4Q1, R-4Q2, and R-4Q11; Reed's collection) in Fig. 5. For each ROI, the BS-SEM image is shown on the left, and the corresponding ternary density plot (relative point density illustrated according to color bar; Fig. 5, bottom left-center) is shown on the right. The distribution of Na-Ca-S ratios throughout the ROI is shown on the right of the ternary density plots (according to the colored ternary diagram at the bottom left of Fig. 5).

Notably, only the ternary diagrams and ratio distribution maps for R-4Q1 show a noteworthy overlap with those of the TS. Specifically, the results show ratios for R-4Q1 that correspond with the theoretical Na-Ca-S ratio of glauberite. Raman measurements collected at an excitation wavelength of 785 nm for R-4Q1 show the presence of sodium sulfate, calcium sulfate, calcite, and, in addition, the peaks associated with the resonant Na_2-X particles, which corroborate the EDS/ternary diagram results (fig. S3). The nitrate peak was not present in the Raman data for the R-4Q1 collagen fibers.

The similarities between the R-4Q1 scroll and the TS are compelling, in that they suggest a potential overlap in their ancient preparation

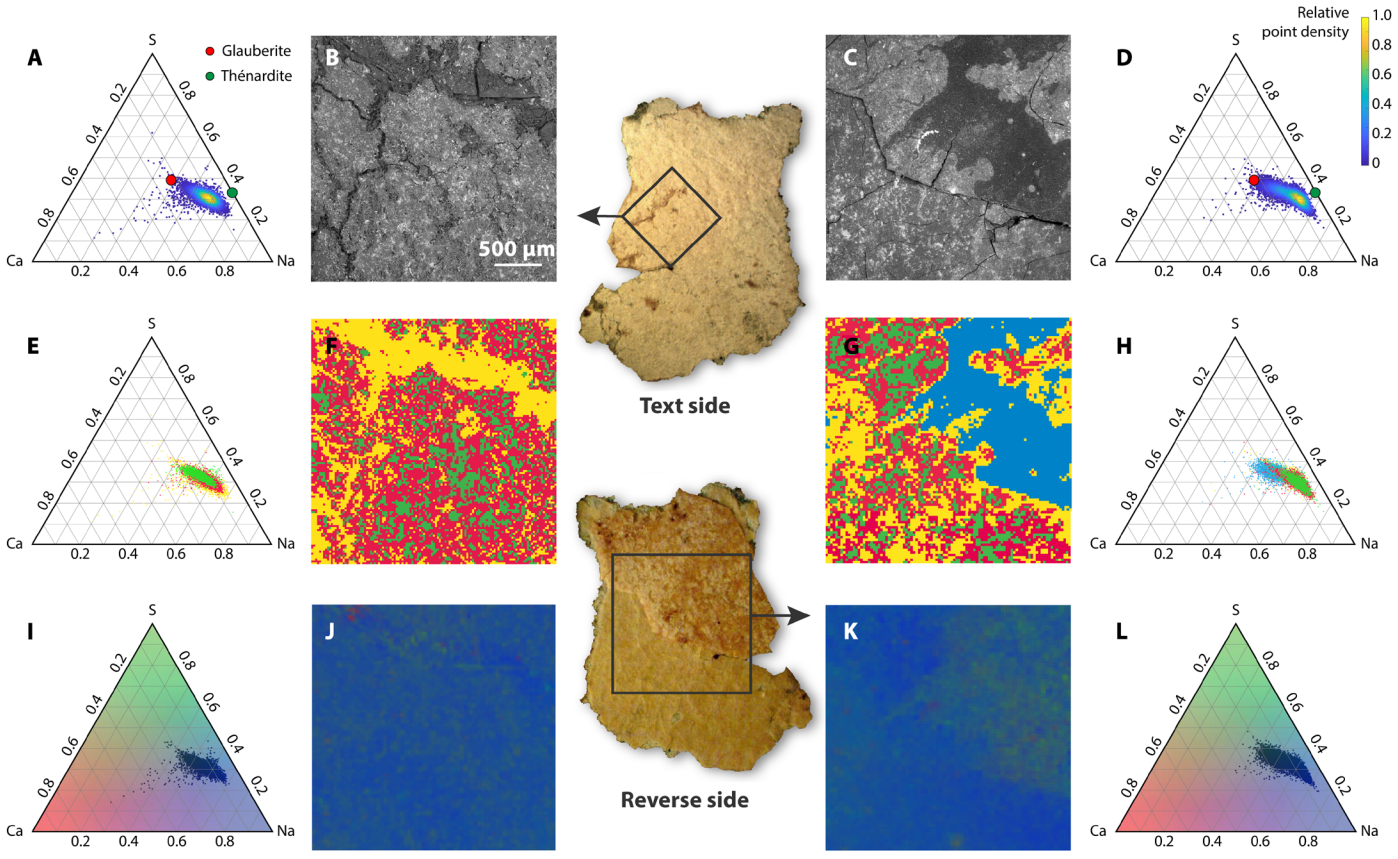

Fig. 4. BS-SEM images, ternary diagrams, and phase maps for the text and reverse sides of the TS. (**A**) Ternary density plot showing Ca-Na-S ratios for a region of the text side, indicated by the box on the optical image (center, top). (**B**) BS-SEM image of a cracked region from the text-containing side of the TS, showing both the inorganic overlayer and the underlying collagenous material. (**C**) BS-SEM image of a region of the reverse side and (**D**) ternary diagram showing the corresponding distribution of Ca-Na-S ratios. Ternary diagrams and phase maps showing the distribution of clustered EDS data for (**E** and **F**) the text side and (**G** and **H**) the reverse side. Ternary diagrams showing the distribution of different Na-S-Ca ratios, colored as RGB combination of the colors at the axes for (**I** and **J**) the text side and (**K** and **L**) the reverse side.

methods, which seem to involve the use of evaporitic salts. Two other scrolls obtained from the same Cave 4Q in Qumran (R-4Q2 and R-4Q11) show ratios of calcium to sodium to sulfur that are significantly different from the TS and the R-4Q1 fragment results, suggesting a different method of production. Although side 2 of R-4Q2 shows a higher concentration of sodium than R-4Q11 and side 1 of R-4Q2, its Na-Ca-S ratios correspond with the ratios of neither glauberite nor thénardite.

DISCUSSION

Among the DSS, the TS is significant because it comprises several anomalies. Its unusual text appears on the flesh side rather than hair side of the exceptionally thin ivory-colored parchment. Previous studies have already pointed at the unusual stratigraphy of the scroll: The text sits on the inorganic layer that covers the extremely thin collagenous base. There are several hypotheses that seek to explain the latter, including the suggestion that the parchment was split into two layers before application of the inorganic layer, but no decisive proof has been offered; therefore, it remains the subject of future research.

Sulfate salts in the inorganic layer

Morphologically, the TS consists of a collagenous organic substrate and a bright, ivory inorganic layer on which the text was written. The present study focused on the characterization of this unique inorganic layer with the objective of understanding the ancient manufacturing technology used to produce the TS, which differs significantly from the other scrolls of the same collection. Using µXRF and EDS, we identified mineral particles rich in Na, Ca, and S, and by applying Raman spectroscopy, the chemical nature of these minerals was determined. The inorganic layer was found to contain a range of minerals, most of which are sulfate salts. Apart from gypsum and its analogs, glauberite [$Na_2Ca(SO_4)_2$] and thénardite (Na_2SO_4) were also identified (*21*). Although the possibility that some of the evaporitic minerals found on the TS may be degradation products of the original inorganic layer cannot be excluded, it is certain that these minerals do not originate from deposition within the caves. The sulfate-containing layers on the surfaces of all of the investigated fragments found on the floors of different Qumran caves have already been studied (*22*), and the mineral sediments on the fragments that were laying on the floors do not match the minerals detected in this study. This result demonstrates the inclusion of the identified evaporitic minerals in the scroll production process.

Comparison of EDS data for TS and Cave 4 fragments

Using large-area EDS data to plot the ratios of the three major elements in glauberite and thénardite (i.e., Ca, Na, and S) on ternary axes allowed the fast assessment of whether parchment samples

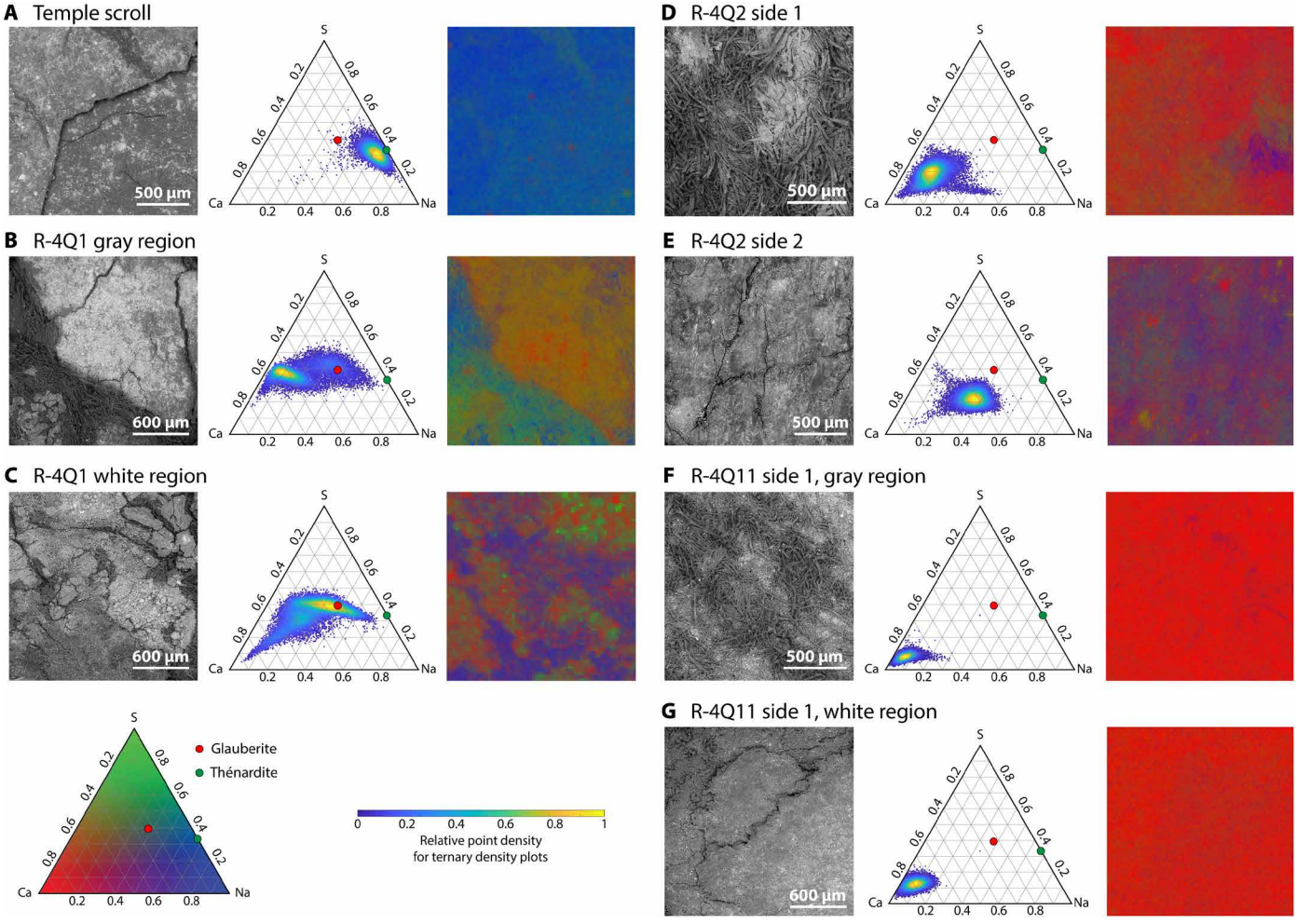

Fig. 5. BS-SEM images, ternary density plots, and Na-S-Ca ratio distribution maps for a subregion of the reverse side of the TS and three additional scrolls obtained from the 4Q cave. Each panel contains the BS-SEM image of the measured regions (left). EDS phase maps were obtained by coloring each pixel according to the ratio of calcium to sodium to sulfur, as indicated by the colored ternary diagram at the bottom left of the figure (center) and ternary density plots, with the relative density of points indicated by the color bar at the bottom left-center of the figure (right).

from Cave 4 (i.e., R-4Q1, R-4Q2, and R-4Q11) might contain similar phases to those found on the TS. R-4Q1 consisted of many data points with Na-Ca-S ratios corresponding to that of glauberite, and upon further analysis with Raman spectroscopy, the presence of the Na_2-X phase was confirmed (fig. S3). Ternary diagrams generated for other fragments from Cave 4 show Na-Ca-S ratios that are similar to each other but different from the TS and R-4Q1. These results suggest that the techniques used to produce the TS may be a part of a larger manufacturing system and that production strategies for the TS and R-4Q1 may share some common features.

Note that the use of ternary diagrams for characterization purposes is not without its limitations. EDS data, because of the relatively low spectral resolution of the technique, is inherently noisy, and data points representing the ratios of the elements when they are only present in trace amounts would show up as noise in the ternary diagrams. For this reason, it was crucial to plot large sets of data on ternary axes because the positions of the centers of clusters of points would indicate the average elemental ratios in a given phase. In addition, because ternary diagrams only account for the ratios of three elements and phases of different chemistries could contain the three elements of interest in the same ratios, it is possible for different phases to occupy the same region of the diagram. This issue could be resolved in a number of ways: The EDS data points could be clustered with respect to several quantified elements (as shown in Fig. 4), or the technique could be used in conjunction with complementary characterization techniques, such as Raman spectroscopy, as was done in this study. In any case, the strength of this technique lies in that it allows the rapid and coarse understanding of the phases present and how they are distributed throughout a sample. In addition, this approach enables the quick comparison of large sets of samples to determine their similarities and differences (as in Fig. 5).

The TS production technology

The Dead Sea brine has a relatively low sulfate concentration, and although these evaporitic salts are particularly common in nonmarine hypersaline environments (*23*), glauberite and thénardite are not commonly found in the Dead Sea region (*24*). This introduces

intriguing questions on the provenance of the TS, which will be the subject of future studies.

Regardless of the origin of the mineral evaporites detected on the TS, their presence in the form of a continuous layer suggests a treatment that differs from the production of other light-colored, untanned (i.e., Western) parchments of the collection, which are represented in the present study by two fragments from Cave 4: R-4Q1 and R-4Q2. The Eastern technology is represented in this study by another Cave 4 fragment: R-4Q11 (*16*). The results of the present study suggest that the inorganic layer of the TS is part of a unique production technology that was applied in antiquity; it differs greatly from the Eastern group but bears similarities to the Western group of parchments. The TS can, therefore, be classified as a Western parchment that was modified through the addition of an inorganic layer as a writing surface. Whether these different technologies were equally implemented in the region for parchment production, however, remains unclear. The link between the production provenance and the applied technology would critically inform the understanding and reconstruction of the technological transfer.

Presence of nitrates in collagen layer

The close association of nitrates and ammonia with the collagen fibers throughout the entire TS fragment is a result of either the parchment production process and the salts used therein or the postproduction degradation/diagenesis of the scroll, for example, during the sojourn in the cave. The former would be possible if evaporitic salts containing nitrates were used in production, but this hypothesis is unsupported by the fact that nitrates were only found in the collagen layer and not in the inorganic mineral layer. We found the degradation/diagenesis hypothesis to be more plausible, considering the traditional degradation pathways of collagen within parchments. It is well understood that artificially aged parchments that are exposed to high concentrations of NO_x gases uptake NO_2, after which NO_3^- ions form within the collagen fibers (*25*–*27*). These ions and their associated radicals might promote the oxidative cleavage of the collagen chains, the byproduct of which is NH_4^+ (*28*). Combined, these two agents would lead to the formation of ammonium nitrate within the TS collagen. Another potential reason for the diagenetic origin of NH_4NO_3 might be related to the presence of bats in Cave 11, which could have affected the microenvironment of the scrolls. The bat excrements (urea and feces) that were ubiquitous in the cave could have led to nitrate enrichment and the subsequent oxidative cleavage described above.

Potential damage due to the presence of hygroscopic salts

Perhaps most critical to our understanding of the TS was the identification of evaporitic sulfate salts in the inorganic layer of this parchment, which places increased emphasis on the close monitoring of environmental conditions that are used for the long-term storage and preservation of these ancient manuscripts. Because of the hygroscopic nature of evaporitic salts, the results presented here highlight their potentially unanticipated sensitivity to even small-scale changes in relative humidity, which could induce volumetric changes in the inorganic phase and increase the concentration of water in contact with the collagen, which may, in turn, accelerate its degradation. In addition to providing insight into the potential degradation pathways of the DSS and the development of methods to slow these processes, the high-throughput nature of the techniques presented here open the door to the rapid, large-scale screening of the remaining thousands of small, and as of yet, unclassified DSS fragments based on their chemical signatures and associated manufacturing methods.

MATERIALS AND METHODS

Confocal Raman spectroscopy

For μ–Raman spectroscopy, a continuous laser beam was focused down to a 1-μm spot on the sample through a confocal Raman microscope (CRM200; WITec, Ulm, Germany) equipped with a piezo-scanner (P-500; Physik Instrumente, Karlsruhe, Germany). The diode-pumped 785-nm near-infrared laser excitation (TOPTICA Photonics AG, Graefelfing, Germany) was used in combination with a 100× (Olympus MPlan IR, 0.95 numerical aperture) objective with approximately 1-μm lateral resolution and approximately 2-μm depth resolution. The spectra were acquired using a charge-coupled device (PI-MAX; Princeton Instruments Inc., Trenton, NJ) behind a grating (300 g mm^{-1}) spectrograph (Acton; Princeton Instruments Inc., Trenton, NJ) with a spectral resolution of ~6 cm^{-1}. Thirty to 60 accumulations with an integration time of 1 s were used for single-spot analyses.

Energy-dispersive x-ray spectroscopy

EDS was used to quantify the elements present on both sides of the TS and in various regions of three scrolls from Cave 4 (R-4Q1, R-4Q2, and R-4Q11). Multidetector EDS was performed using a TESCAN VEGA GMU SEM equipped with two Bruker XFlash 5030 x-ray detectors. Mapping data were acquired at a 15-mm analytical working distance at an accelerating voltage of 20 keV. Each EDS dataset was quantified using bins of 9 pixels by 9 pixels to improve the statistics for quantification to yield elemental concentrations present at each pixel. The quantification of EDS data was performed with Bruker's ESPRIT 2.1 software using the built-in Linemarker PB-ZAF correction, which corrected for background radiation, atomic number effects, absorption of x-rays by the specimen, and fluorescence. The single-element quantified EDS maps were processed using custom MATLAB scripts to produce the ternary diagrams presented.

The quantified EDS data were also processed using fuzzy c-means clustering (Fuzzy Logic Toolbox, MATLAB R2018a), in which each data point could be a part of a number of clusters and, hence, is assigned a membership value for each cluster. Custom MATLAB software was written to segment the data points based on the clusters for which they had the highest membership value. Clustering was carried out with respect to the four major elements that were quantified for each dataset: sodium, calcium, sulfur, and iron.

FT-Raman spectroscopy

To obtain Raman measurements for average, representative regions of samples that usually exhibit strong background fluorescence, a Bruker FT-Raman spectrophotometer (RFS 100/S) was used. The instrument was equipped with a Ge-diode detector cooled with liquid nitrogen (77 K), and a near-infrared (YAG:Nd) laser operating at 1064 nm. Measurements were carried out with a laser output power of 50 to 100 mW, and spectra were collected in the spectral range of 100 to 3600 cm^{-1} with a spectral resolution of 4 cm^{-1}. A total of 4000 scans were co-added per spectrum. The spot size of the beam on the sample was approximately 400 μm in diameter.

μXRF spectroscopy (TORNADO)

A tabletop Bruker 2D μXRF spectrometer (M4 TORNADO) was used to obtain detailed, spatially resolved elemental maps of large sample surface areas. The probe contained an air-cooled, low-power Rh ($K\alpha_1$ = 20.2 keV) x-ray tube, operated at 50 kV and 600 μA, with polycapillary x-ray optics and an electrothermally cooled XFlash detector. The spectrometer was evacuated to enhance the detection of light elements. Major improvements in data collection included the use of a small measurement spot of 25 μm and a high-speed *x-y* sample stage. The fluorescence signal was measured continuously while the stage moved with predefined step sizes.

Sample collection

Samples R-4Q1, R-4Q2, and R-4Q11 were donated by the Rylands Library of Manchester University and were part of the original collection of the nontreated samples supplied to R. Reed for material analysis in 1956. The samples of the TS were supplied by the Shrine of the Book, and the sample mounting methods used were chosen to minimize sample degradation during noninvasive data acquisition.

SUPPLEMENTARY MATERIALS

Supplementary material for this article is available at http://advances.sciencemag.org/cgi/content/full/5/9/eaaw7494/DC1

Fig. S1. Schematic showing the stratigraphy of the TS fragment, 11QT[a].

Fig. S2. Raman (785 nm) spectra of TS inorganics and related sulfate salts.

Fig. S3. Raman (785 nm) spectra showing the detected components of the R-4Q1 scroll and reference spectra for gypsum and thénardite.

REFERENCES AND NOTES

1. L. Bertrand, C. Gervais, A. Masic, L. Robbiola, Paleo-inspired systems: Durability, sustainability, and remarkable properties. *Angew. Chem. Int. Ed.* **57**, 7288–7295 (2018).
2. Z. de Groot, in *Pergament—Geschichte, Struktur, Restaurierung und Herstellung heute*, P. Rück, Ed. (Jan Thorbecke, 1992).
3. J. B. Poole, R. Reed, The preparation of leather and parchment by the dead sea scrolls community. *Technol. Cult.* **3**, 1–26 (1962).
4. A. Wallert, in *ICOM Committee for Conservation: 11th Triennial Meeting in Edinburgh, Scotland, 1-6 September 1996: Preprints* (James & James, 1996), pp. 560–564.
5. Inden witten Hasewint; http://indenwittenhasewint.blogspot.com/.
6. R. Reed, *Ancient Skins, Parchments and Leathers* (Seminar Press, 1972).
7. Y. Yadin, *Tefillin from Qumran* (Israel Exploration Society, 1969), vol. 9, pp. 60–85.
8. I. Rabin, O. Hahn, Characterization of the Dead Sea Scrolls by advanced analytical techniques. *Anal. Methods* **5**, 4648–4654 (2013).
9. I. Rabin, in *Jewish Manuscript Cultures: New Perspectives* (Walter de Gruyter GmbH & Co KG, 2017), vol. 13.
10. Y. Yadin, The Temple Scroll. *Biblic. Archaeol.* **30**, 135–139 (1967).
11. I. Rabin, in *Gleanings from the Caves. Dead Sea Scrolls and Artefacts of The Schøyen Collection*, T. Elgyin, K. Davis, M. Langlois, Eds. (Bloomsbury T&T Clark, 2016), pp. 327–338.
12. H. J. Plenderleith, *Discoveries in the Judean Desert I, Qumran Cave I* (1955), pp. 39–40.
13. Y. Yadin, *The Temple Scroll: The Hidden Law of the Dead Sea Sect* (Random House Incorporated, 1985).
14. S. Weiner, Z. Kustanovich, E. Gil-Av, W. Traub, Dead sea scroll parchments: Unfolding of the collagen molecules and racemization of aspartic acid. *Nature* **287**, 820–823 (1980).
15. M. Derrick, Evaluation of the state of degradation of Dead Sea Scroll samples using FT-IR spectroscopy, in *The Book and Paper Group Annual* (Book and Paper Group, 1991), vol. 10, pp. 49–65.
16. R. Schütz, L. Bertinetti, I. Rabin, P. Fratzl, A. Masic, Quantifying degradation of collagen in ancient manuscripts: The case of the Dead Sea Temple Scroll. *Analyst* **138**, 5594–5599 (2013).
17. M. Bicchieri, A. Sodo, I. Rabin, A. Kohl, G. Piantanida, New results in Dead Sea Scrolls non-destructive characterisation. Evidence of different parchment manufacture in the fragments from Reed collection. *J. Cult. Herit.* **32**, 22–29 (2018).
18. J. B. Poole, thesis, University of Leeds (1960).
19. R. A. Nyquist, R. O. Kagel, *Handbook of Infrared and Raman Spectra of Inorganic Compounds and Organic Salts: Infrared Spectra of Inorganic Compounds* (Academic Press, 2012).
20. B. Lafuente, R. T. Downs, H. Yang, N. Stone, in *Highlights in Mineralogical Crystallography*, T. Armbruster, R. M. Danisi, Eds. (De Gruyter, 2015), pp. 1–30.
21. Mineral Data Publishing, "Glauberite"; http://rruff.info/doclib/hom/glauberite.pdf.
22. T. Wolff, I. Rabin, I. Mantouvalou, B. Kanngießer, W. Malzer, E. Kindzorra, O. Hahn, Provenance studies on Dead Sea scrolls parchment by means of quantitative micro-XRF. *Anal. Bioanal. Chem.* **402**, 1493–1503 (2012).
23. S. Boggs Jr., *Principles of Sedimentology and Stratigraphy* (Pearson Education, 2014).
24. R. A. Garber, Y. Levy, G. M. Friedman, The sedimentology of the Dead Sea. *Carbonates Evaporites* **2**, 43–57 (1987).
25. E. Badea, L. Miu, P. Budrugeac, M. Giurginca, A. Mašić, N. Badea, G. D. Gatta, Study of deterioration of historical parchments by various thermal analysis techniques complemented by SEM, FTIR, UV-Vis-NIR and unilateral NMR investigations. *J. Therm. Anal. Calorim.* **91**, 17–27 (2008).
26. S. Boghosian, Structural damage of parchment at the molecular level assessed by Raman spectroscopy, in *Improved Assessment of Parchment*, R. Larsen, Ed. (Office for Official Publications of the European Communities, 2007), pp. 105–109.
27. R. Larsen, D. Poulsen, F. Juchauld, H. Jerosch, M. Odlyha, J. de Groot, Q. Wang, C. Theodorakopoulos, T. Wess, J. Hiller, C. Kennedy, G. Della Gatta, E. Badea, A. Mašić, S. Boghosian, D. Fessas, Damage assessment of parchment: Complexity and relations at different structural levels, in *ICOM-CC, 14th Triennial Meeting, 12-16 September 2005, The Hague* (ICOM-CC, 2005), vol. 1, pp. 199–208.
28. C. J. Kennedy, T. J. Wess, The structure of collagen within parchment—A review. *Restaurator* **24**, 61–80 (2003).
29. Digital Dead Sea Scrolls at the Israel Museum, Jerusalem—The Temple Scroll; http://dss.collections.imj.org.il/temple.

Acknowledgments: We thank the John Rylands Library and the Shrine of the Book for permission to study the fragments. We would like to thank P. Fratzl for invaluable insights throughout this work through frequent and meaningful discussions. We would also like to thank R. Tagle for support in the collection of μXRF measurements collected using TORNADO instrumentation at Bruker. We also thank M. Stämmler, P. Lasch (RKI, Berlin), and A. Kohl (BAM, Berlin) for support in conducting FT-Raman measurements. **Funding:** Funding from the DFG is gratefully acknowledged. **Author contributions:** A.M. and I.R. conceived the idea and designed the study. A.M. supervised the study. R.S. performed light microscopy and confocal Raman microspectroscopy data acquisition and data processing. R.S. and I.R. performed FT-Raman and μXRF experiments and interpreted results. J.M.M. and J.C.W. performed SEM-EDS acquisition, data processing, and interpretation of results. J.M.M. performed EDS data clustering and ternary diagram analysis. J.C.W. performed large-area BS-SEM imaging. A.M. drafted the manuscript with inputs from all other authors. **Competing interests:** The authors declare that they have no competing interests. **Data and materials availability:** All data needed to evaluate the conclusions in the paper are present in the paper and/or the Supplementary Materials. Raw data files are available at: https://doi.org/10.6084/m9.figshare.8192366.v1. Additional data related to this paper may be requested from the authors.

Submitted 23 January 2019
Accepted 12 August 2019
Published 6 September 2019
10.1126/sciadv.aaw7494

Citation: R. Schuetz, J. M. Maragh, J. C. Weaver, I. Rabin, A. Masic, The Temple Scroll: Reconstructing an ancient manufacturing practice. *Sci. Adv.* **5**, eaaw7494 (2019).

ScienceAdvances

The Temple Scroll: Reconstructing an ancient manufacturing practice

Roman Schuetz, Janille M. Maragh, James C. Weaver, Ira Rabin and Admir Masic

Sci Adv **5** (9), eaaw7494.
DOI: 10.1126/sciadv.aaw7494